DksA regulates RNA polymerase in *Escherichia coli* through a network of interactions in the secondary channel that includes Sequence Insertion 1

Andrey Parshin[a,b,1], Anthony L. Shiver[c,1], Jookyung Lee[a], Maria Ozerova[a,2], Dina Schneidman-Duhovny[d], Carol A. Gross[e,f,g,3], and Sergei Borukhov[a,3]

[a]Department of Cell Biology, Rowan University School of Osteopathic Medicine at Stratford, Stratford, NJ 08084-1489; [b]Graduate School of Biomedical Studies, Rowan University School of Osteopathic Medicine at Stratford, Stratford, NJ 08084-1489; [c]Graduate Group in Biophysics, University of California, San Francisco, CA 94158; [d]Department of Bioengineering and Therapeutic Sciences, University of California, San Francisco, CA 94158; [e]Department of Microbiology & Immunology, University of California, San Francisco, CA 94143-001; [f]Department of Cell and Tissue Biology, University of California, San Francisco, CA 94143-001; and [g]California Institute of Quantitative Biology, University of California, San Francisco, CA 94143-001

Contributed by Carol A. Gross, November 1, 2015 (sent for review September 9, 2015; reviewed by Seth A. Darst and Richard L. Gourse)

Sensing and responding to nutritional status is a major challenge for microbial life. In *Escherichia coli*, the global response to amino acid starvation is orchestrated by guanosine-3′,5′-bisdiphosphate and the transcription factor DksA. DksA alters transcription by binding to RNA polymerase and allosterically modulating its activity. Using genetic analysis, photo–cross-linking, and structural modeling, we show that DksA binds and acts upon RNA polymerase through prominent features of both the nucleotide-access secondary channel and the active-site region. This work is, to our knowledge, the first demonstration of a molecular function for Sequence Insertion 1 in the β subunit of RNA polymerase and significantly advances our understanding of how DksA binds to RNA polymerase and alters transcription.

transcription regulation | stringent response | protein cross-linking | molecular modeling | lineage-specific insertions

Sensing and responding to nutritional status is one of the major challenges of microbial life. In *Escherichia coli*, the global regulatory response to amino acid starvation is orchestrated by the second messenger guanosine-3′,5′-bisdiphosphate (ppGpp), which is a widely conserved master regulator (1). Accumulation of ppGpp during amino acid scarcity triggers the stringent response, which down-regulates expression of rRNA and tRNA while increasing expression of amino acid biosynthetic enzymes. In *E. coli*, ppGpp works synergistically with the transcription factor DksA to initiate the stringent response (2, 3). Both ppGpp and DksA are critical for survival of stress and virulence in many pathogenic proteobacteria (4).

DksA is a relatively small protein with a prominent N-terminal coiled-coil domain and a globular C-terminal domain consisting of a Zn^{2+}-binding region and a C-terminal α-helix (3). It belongs to a class of regulators that bind directly to RNA polymerase (RNAP) without contacting DNA (5). DksA modulates RNAP activity by preventing formation of or destabilizing the intermediate complex (RPi) on the pathway to the open complex (RPo), which is competent for initiation. For promoters with intrinsically unstable open complexes, such as rRNA promoters, DksA binding leads to decreased transcription (2).

DksA is a critical determinant of the stringent response and a model system for an important class of transcription regulators, making it essential to understand how DksA interacts with RNAP at the molecular level. High-resolution structural information of the DksA/RNAP interaction is currently unavailable. Current models agree that the coiled-coil domain of DksA inserts into the secondary channel of RNAP, the channel used by NTPs to access the active site; that the secondary channel rim helices of β' subunit are critical for DksA binding; and that residues at the tip of the coiled-coil of DksA are important for its activity. However, the precise placement of DksA is unknown. With the number of critical features that can be accessed through the secondary channel, even small changes in the model can significantly change the details of the interaction and mechanistic interpretation, making it imperative to determine the DksA position more precisely.

Using both chemical-genomic and high-resolution mapping of site-specific cross-links, we have discovered previously unidentified features of RNAP that are essential for DksA binding and activity. Motivated by these novel findings, we have integrated information from cross-link mapping and extensive mutagenesis coupled to functional assays to revisit the model of DksA bound to RNAP, resulting in the highest resolution model of DksA binding to date. We identify β subunit Sequence Insertion 1 (β-SI1) as a binding site for DksA and describe evidence for a bipartite binding site comprised of β-SI1 and the conserved β' rim helices. We also show that the tip of DksA interacts with the highly conserved substrate-binding region of the β subunit active site. This work advances our mechanistic understanding of DksA activity in *E. coli* and expands our knowledge of the evolutionary conservation of transcription regulation by DksA and ppGpp.

Results

A Chemical-Genomic Screen Illuminates a Connection Between β-SI1 and DksA. A chemical-genomic screen of a large library of chromosomal

Significance

The transcription factor DksA is a critical determinant of the stringent response and is essential for virulence in many pathogenic proteobacteria. This ubiquitous transcription factor is also a model system for transcription regulation, making it essential to understand how DksA interacts with RNA polymerase (RNAP) at the molecular level. High-resolution structural information of the DksA–RNAP interaction is currently unavailable. Using genetic, biochemical, and computational approaches, we have generated a new high-quality model of the DksA–RNAP interaction that advances our understanding of DksA binding and activity and will serve as a springboard for future mechanistic investigations into DksA regulation.

Author contributions: A.P., A.L.S., C.A.G., and S.B. designed research; A.P., A.L.S., J.L., M.O., D.S.-D., and S.B. performed research; A.P., A.L.S., J.L., M.O., D.S.-D., C.A.G., and S.B. analyzed data; and A.P., A.L.S., C.A.G., and S.B. wrote the paper.

Reviewers: S.A.D., The Rockefeller University; and R.L.G., University of Wisconsin-Madison.

The authors declare no conflict of interest.

[1]A.P. and A.L.S. contributed equally to this work.

[2]Present address: The Wistar Institute, Philadelphia, PA 19104.

[3]To whom correspondence may be addressed. Email: borukhse@rowan.edu or cgrossucsf@gmail.com.

This article contains supporting information online at www.pnas.org/lookup/suppl/doi:10.1073/pnas.1521365112/-/DCSupplemental.

RNAP mutants against many chemical conditions found that an RNAP mutant lacking the β-SI1 insertion, *rpoB(ΔSI1)*, had a clear growth defect during amino acid starvation. This defect was manifested both when amino acids were omitted from the media and when starvation was mimicked with serine hydroxamate (SHX–), which prevents amino-acylation of seryl-tRNA (Fig. 1*A*). This phenotype is similar to that of Δ*dksA*, which led us to further compare their phenotypes.

The amino acid requirements of *ΔdksA* and *rpoB(ΔSI1)* are equivalent. Both strains grew slowly when deprived of amino acids but were not true auxotrophs, as colonies became visible after 2 days of growth (Fig. 1*B*). Moreover, the same set of amino acids (the Σ-set, DQILVFHST) (6) is sufficient to complement the amino acid requirements of both *ΔdksA* and *rpoB(ΔSI1)* (Fig. 1*B*). Finally, sequencing of suppressors that restored prototrophy to *rpoB(ΔSI1)* identified two mutations in RNAP already known to suppress the amino acid requirements of *ΔdksA* and ppGpp^0: *rpoB(P153L)* and *rpoC(Δ215–220)* (Fig. 1*C*) (7–9). The similarity of *rpoB(ΔSI1)* and *ΔdksA* across a battery of tests suggested the two mutations may have similar effects on transcription. This led us to speculate that β-SI1, located near DksA in models of the RNAP/DksA complex, is a previously unappreciated DksA-binding site.

Bpa Cross-Linking Probes Reveal the Proximity of DksA to β in the Complex. To map RNAP sites in close proximity to DksA, we incorporated p-benzoyl-p-phenylalanine (Bpa) into 24 surface-exposed residues of DksA, covering all of its structural features (Fig. 2*A*). UV light activates Bpa to cross-link nearby alkyl carbons with a preference for aliphatic residues (10). Bpa substitutions provide highly specific cross-linking information that can resolve unique binding partners in nearby features (11). We tested each purified, radiolabeled variant for cross-linking to RNAP holoenzyme in vitro, identifying 18 variants that cross-linked to one of the two large subunits in RNAP (*SI Appendix*, Fig. S1). We distinguished cross-linking to β or β' by cross-linking unlabeled DksA-Bpa variants to RNAP radiolabeled in either the β or β' subunit (Fig. 2*B*). Thirteen DksA-Bpa variants preferentially cross-linked to β', as expected from earlier results that identified β' as a cross-linking partner of DksA (12), and five preferentially cross-linked to β (Fig. 2 *B* and *C*). To our knowledge, this was the first evidence that β contributes to DksA binding.

We mapped the cross-link sites in β and β' to greater resolution, using limited cyanogen bromide (BrCN) cleavage, which cleaves after methionine residues. The BrCN cleavage patterns of RNAP subunits are well-established (13, 14), allowing for clear assignment of cross-link adducts to fragments of the large subunits (*SI Appendix*, Fig. S2*A*). In some cases, we further refined the cross-linking region by enzymatically cleaving the cross-linked products with trypsin under single-hit conditions. In total, we located cross-link sites on β and β' for 11 DksA-Bpa variants to a precision of 10–50 residues (*SI Appendix*, Fig. S2 *B–K*). The results, summarized in Fig. 2*D* and *SI Appendix*, Fig. S3 *A–D*, identified eight new cross-linking sites and increased the precision of three previously identified sites (DksA F69, E79, and E146) by an order of magnitude (12). DksA-Bpa cross-links mapped to two new regions in β that were not predicted by current models: a region overlapping β-SI1 and one that included a substrate-binding region from β. This motivated us to revisit the structural model of DksA bound to RNAP.

A New Evidence-Based Model for the DksA–RNAP Complex. We first sought to understand the general constraints on possible models of DksA and RNAP imposed by our new cross-linking data. For this purpose, we used computational docking with PatchDock (15) to generate nearly 130,000 different models of DksA bound to RNAP using two constraints: We required that the interface between the two structures satisfied shape complementarity rules and that at least one of the mapped cross-link regions contacted DksA directly. This set was then filtered using distance constraints from the cross-links (distance in structure < 20 Å). Simultaneous satisfaction of seven cross-link constraints filtered the set to just three similar docking solutions (rmsd, <11 Å) sharing two prominent features. First, the tip of DksA inserted deep into the secondary channel and approached the substrate-binding site in the β subunit. Second, the C-terminal α-helix of DksA extended out toward β-SI1 in the secondary channel. Of the three docking positions, two positions placed the globular

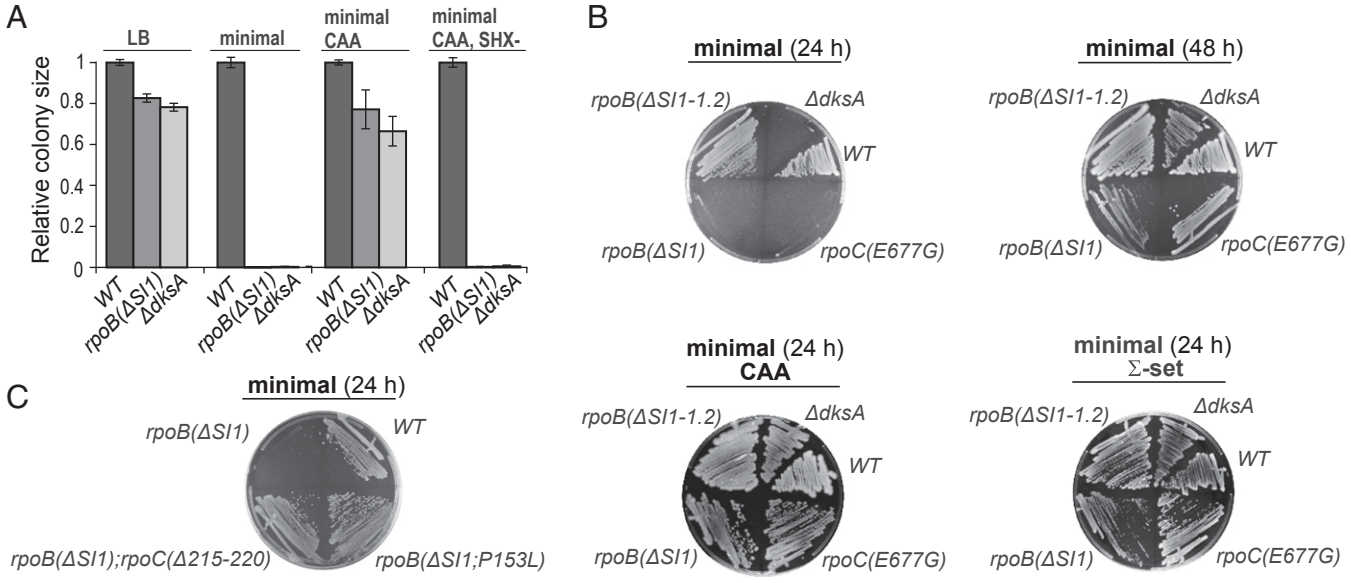

Fig. 1. β-SI1 is critical for growth during amino acid limitation. (*A*) Quantification of colony sizes of the WT and mutant *E. coli* strains [*rpoB(ΔSI1)* and *ΔdksA*] grown under the indicated conditions. Colony sizes are normalized to the WT strain for each condition. Error bars represent SDs ($n > 3$). CAA, casamino acids; SHX-, serine hydroxamate. (*B*) Growth phenotypes of *rpoB(ΔSI1)* during amino acid limitation. The Σ-set of amino acids is comprised of D, Q, I, L, V, F, H, S, and T. (*C*) Spontaneous suppressors of *rpoB(ΔSI1)*, *rpoC(Δ215–220)*, and *rpoB(P153L)* restore growth during amino acid limitation.

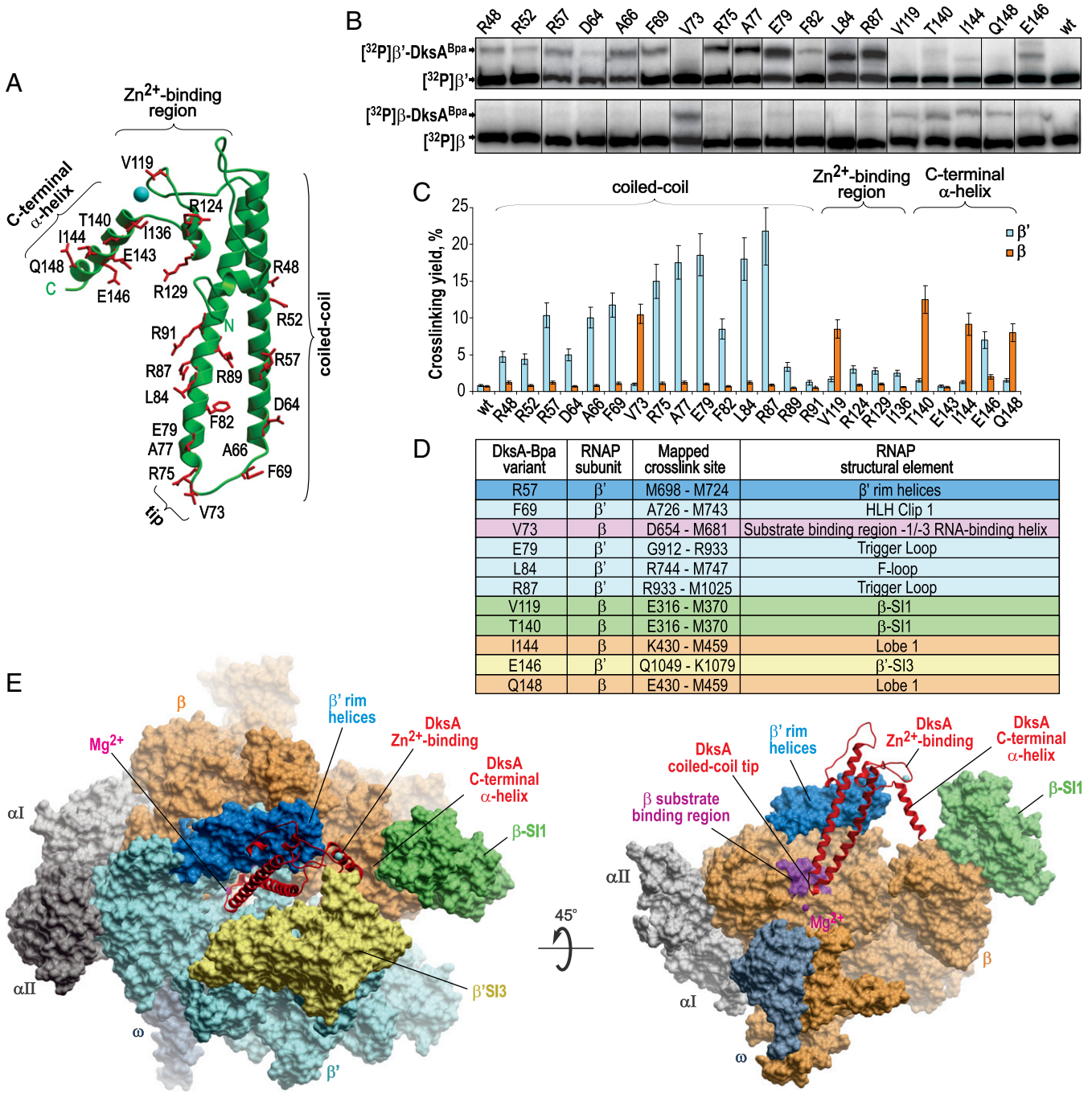

DksA-Bpa variant	RNAP subunit	Mapped crosslink site	RNAP structural element
R57	β'	M698 - M724	β' rim helices
F69	β'	A726 - M743	HLH Clip 1
V73	β	D654 - M681	Substrate binding region -1/-3 RNA-binding helix
E79	β'	G912 - R933	Trigger Loop
L84	β'	R744 - M747	F-loop
R87	β'	R933 - M1025	Trigger Loop
V119	β	E316 - M370	β-SI1
T140	β	E316 - M370	β-SI1
I144	β	K430 - M459	Lobe 1
E146	β'	Q1049 - K1079	β'-SI3
Q148	β	E430 - M459	Lobe 1

Fig. 2. Probing of DksA–RNAP spatial organization by Bpa cross-linking. (*A*) Ribbon structure of *E. coli* DksA (PDB ID code 1TJL) indicating its structural features and the positions of the 24 residues substituted with Bpa (red sticks). (*B*) Autoradiograms of photo–cross-linked DksA-Bpa variants to the RNAP core having either radiolabeled β′ (*Top*) or β (*Bottom*). The position of cross-linked variants and free subunits is indicated by arrows. (*C*) Cross-linking yield of each DksA-Bpa variant to β′ (cyan bars) and β (orange bars) with SD ($n = 3$) indicated. (*D*) Summary of the mapped cross-linked sites, color-coded to match the RNAP regions shown in *E*. Structural elements listed are described in ref. 37. (*E*) Structural model of the DksA–RNAP complex. (*Left*) Secondary channel surface view of *E. coli* RNAP holoenzyme (PDB ID code 4LK1) (αI, light gray; αII, gray; β, orange; β′, cyan; ω, slate gray; σ is omitted for clarity) in complex with *E. coli* DksA (PDB ID code 1TJL), which is shown as a red ribbon with structural features indicated by arrows. The view emphasizes the position of DksA relative to three secondary channel domains: β-SI1 (light green), β′-SI3 (light yellow), and β′ rim helices (blue). (*Right*) Rotation by ∼45° with β′ surface removed to reveal the position of the DksA coiled-coil tip relative to the β subunit substrate-binding region. The −1/−3 RNA-binding helix (βD675-M681) and the NTP-binding loop (βS1105-N1108) are colored purple; the catalytic Mg^{2+} ion is a dark purple ball.

domain of DksA closer to the β' jaw domain (β'1147–1245), whereas only one positioned the globular domain of DksA closer to the tip of the β' rim helices, a known binding determinant of DksA (12, 16). We used this solution for further refinement of the structural model. Notably, the best docking solution was still limited by a steric clash between the rim helices and the N terminus of DksA, a structural feature that has been demonstrated to be dispensable for DksA function (16).

To create a refined model of DksA bound to RNAP that reflected residue-level information on the interaction, we used

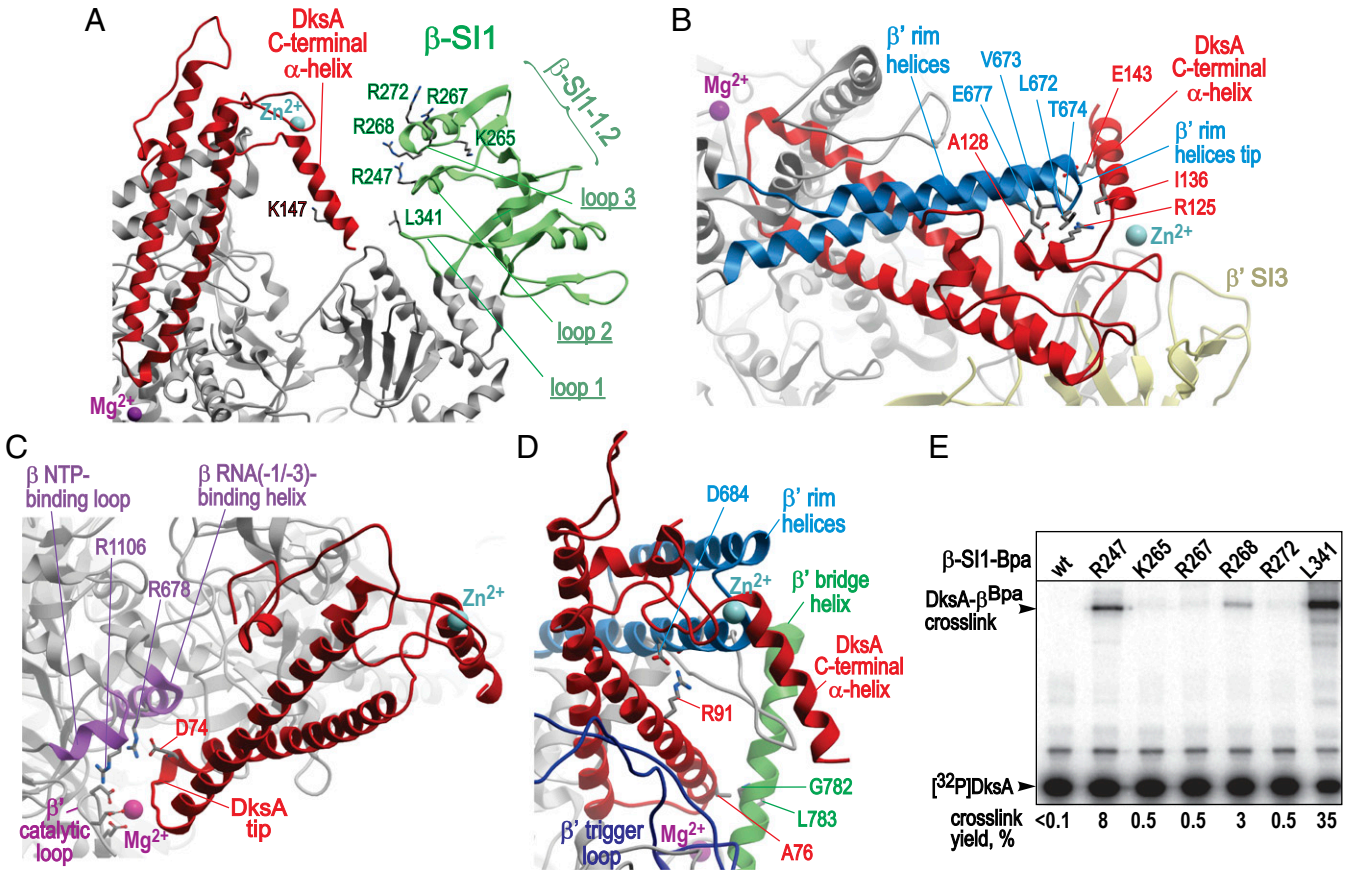

Fig. 3. Detailed views of the structural model of the DksA–RNAP complex. (*A*) Structural view of possible interactions between the DksA C-terminal α-helix and β-SI1. Residues with Bpa substitutions in β-SI1 loops 1, 2, and 3 are depicted as sticks. (*B*) DksA Zn^{+2}-binding region and β′ rim helix tips; in this and the following panels, critical contacts are depicted as sticks. (*C*) DksA coiled-coil tip residue D74 and β active-site region NTP-binding loop/RNA (–1/–3)-binding helix. (*D*) DksA coiled-coil residue R91 and β′ rim helix residues encompassing D684, DksA-A76, and β′ bridge helix residues G782/L783. The panel is color-coded as in Fig. 2*E*, except for the β′ bridge helix (green) and the β′ TL (dark blue; open conformation as in PDB ID code 3LU0). (*E*) Autoradiogram of photo–cross-linking between WT DksA and RNAPs carrying six different Bpa substitutions in β-SI1.

additional experimental information based on the functional characterization of ≥30 point mutants and several partial deletions (Figs. 2–6 and *SI Appendix*, Figs. S4–S6). We positioned DksA within the secondary channel so that functionally relevant residues made reasonable contacts in the interface. Importantly, only minor changes in the orientation and position of DksA in the automated model (rmsd, 7 Å) were necessary (*SI Appendix*, Fig. S3*E*). The final model (Fig. 2*E* and model 3 in *SI Appendix*, Fig. S3*E*) suggests four likely interaction sites between DksA and RNAP: the DksA C-terminal α-helix and β-SI1 (Fig. 3*A*), the DksA Zn^{2+}-binding domain and adjacent C-terminal α-helix with the tip of the β' rim helices (Fig. 3*B*), DksA residue D74 with residues in the β substrate-binding region (Fig. 3*C*), and the middle of the DksA coiled-coil domain with the β' N-terminal rim helix (Fig. 3*D*).

β-SI1 Interacts with DksA. Consistent with the functional connection between β-SI1 and DksA discovered in our chemical-genomic screen, two DksA-Bpa adducts, DksA-V119Bpa and DksA-T140Bpa, mapped to a region of β overlapping with SI1 (Fig. 2*D*). We independently confirmed the physical proximity of DksA and β-SI1 in the bound complex using a "reciprocal" cross-linking experiment, showing that two β-SI1–Bpa derivatives, β-L341Bpa and β-K247Bpa, cross-linked to DksA with high efficiency (Fig. 3*E*). These reciprocal cross-links are strong evidence of the proximity of β-SI1 and DksA in the complex.

The β-SI1-1.2 (β-240–284) subdomain of β-SI1 faces the secondary channel and is oriented toward DksA in the model—with loops 2 (β-E244-S252) and 3 (β-G266-R272) positioned as possible interfaces with DksA (Fig. 3*A*). Consistent with this prediction, both RNAPΔSI1 and RNAPΔSI11.2 mutant polymerases had dramatically decreased DksA-dependent inhibition of transcription from *rrnBP1* (Fig. 4*A*) and DksA binding in vitro (Fig. 4*B*). Moreover, multiple-alanine substitutions in both loop 2 and loop 3 of β-SI1-1.2 significantly decreased DksA binding and inhibitory activity in vitro (*SI Appendix*, Table S1 and Fig. S9). Additionally, both *rpoB(ΔSI1)* and *rpoB(ΔSI1-1.2)* exhibited a phenotype in vivo, failing to repress transcription from a reporter construct driven from an *rrnBP1* promoter during stationary phase growth. Loss of repression was similar in magnitude to that of Δ*dksA* and *rpoC(E677C)*, a mutant in the β' rim helices that mimics the in vivo phenotypes of Δ*dksA* (Fig. 4*C*) (17). Importantly, this effect was not due to a general transcriptional defect of *rpoB(ΔSI1)* or *rpoB(ΔSI1-1.2)*: Both deletion strains showed less than a twofold increase in expression of *lacUV5-lacZ*, comparable to that described for Δ*dksA* (18) (Fig. 4*C*). The defect of RNAPΔSI1-1.2 in repressing transcription either in vivo or in vitro was only slightly less than that of *rpoB(ΔSI1)*. However, *rpoB(ΔSI1-1.2)* was less defective than *rpoB(ΔSI1)* during growth without amino acids, as the strain suffered no lag and showed only a small (~30%) reduction in colony size relative to WT (Fig. 4*D* and *SI Appendix*, Fig. S8). The discrepancy in the severity of phenotypes detected by these assays could be explained by their relative sensitivities or by differences in conditions. The binding defect of *rpoB(ΔSI1-1.2)* may not be sufficient to disrupt growth without amino acids, or

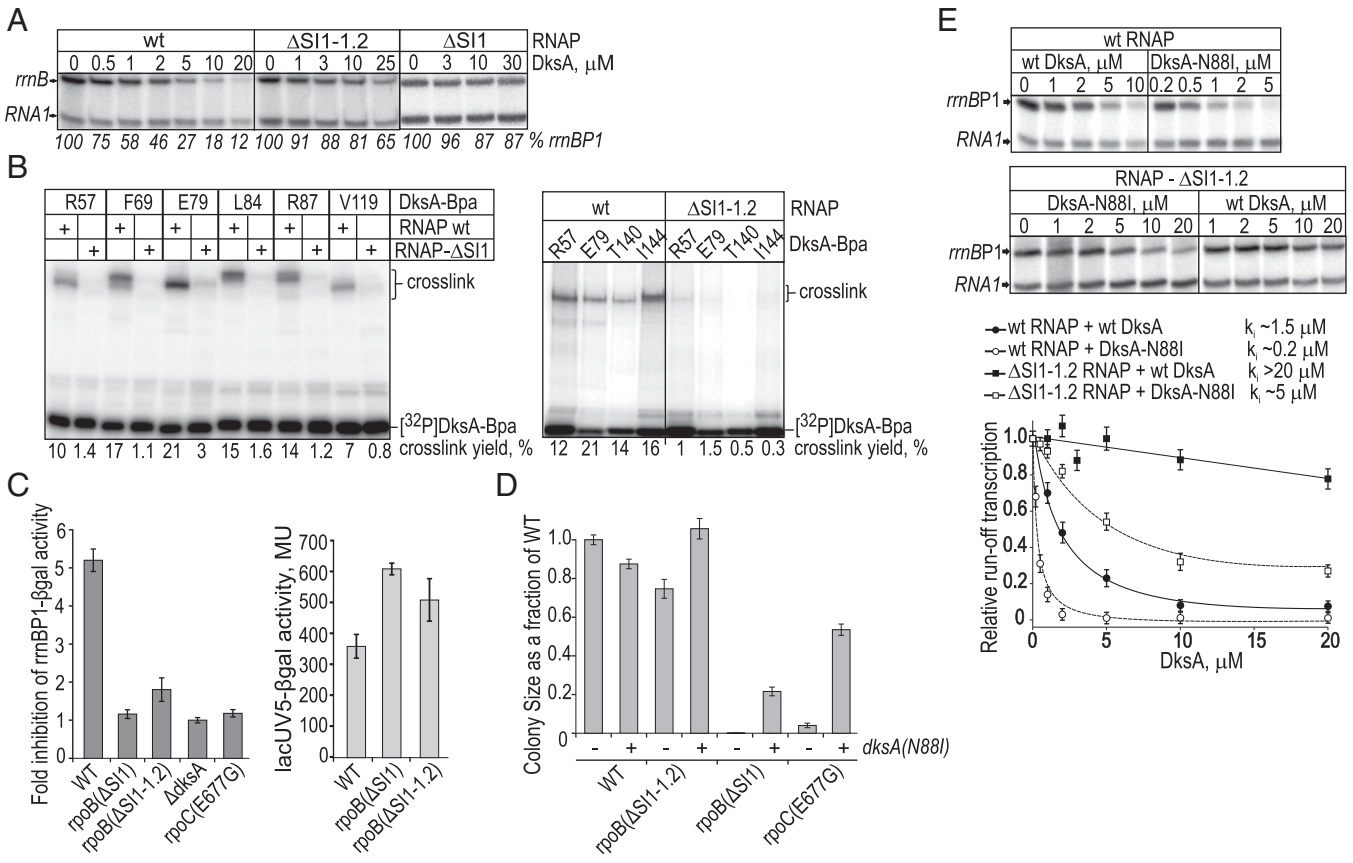

Fig. 4. Comparison of the phenotypes of RNAP Δβ-SI1 and Δβ-SI1-1.2. (*A*) Multiround transcription assays (2) comparing the concentration dependence of DksA inhibition of *rrnBP1* transcription initiated by WT RNAP (*Left*), β-ΔSI1 RNAP (*Center*), or β-ΔSI1-1.2 RNAP (*Right*). The percentage of terminated *rrnBP1* transcripts made with DksA relative to that without DksA is indicated below each lane of the gel autoradiogram. (*B*) Autoradiograms of 6–12% SDS/PAGE of different DksA-Bpa photo–cross-linked to WT or mutant RNAP β-ΔSI1 (*Left*) and to β-ΔSI1-1.2 (*Right*). Cross-linking yield is indicated below each lane. (*C*) Stationary phase inhibitory activity of DksA in strains with β-ΔSI1 and β-ΔSI1-1.2 mutations (derivatives of RLG5920, RLG4764, and RLG5022; see *SI Appendix*, Table S6). (*Left*) Fold inhibition of *rrnB-P1* activity relative to that in a strain lacking DksA, assayed using an *rrnBP1*–β-gal fusion reporter strain and measured 24 h after inoculation. (*Right*) Activity of WT and β-SI1 variants on a *lacUV5*–β-gal fusion reporter measured 24 h after inoculation. (*D*) The fitness defect of *rpoB(ΔSI1)* on minimal media is partially suppressed by *dksA(N88I)* (derivatives of BW25113; see *SI Appendix*, Table S6). Colonies were pinned onto minimal media, and colony size was quantified and normalized to WT. Error bars reflect SD ($n > 3$). (*E*, *Left*) Same as in *A* except that reactions used the hyperactive DksA mutant, DksA-N88I. (*E*, *Right*) Quantification of the concentration dependence of DksA inhibitory activity in various strains from which k_i is calculated.

the elevated ppGpp levels during amino acid starvation could complement any partial defects through synergy with DksA (2).

The model predicted that the C-terminal α-helix of DksA spanned the junction from the β' rim helices to β-SI1, with residues that could be reasonably expected to interact with either feature, motivating us to identify any DksA residues that could contribute to these interfaces. As previously reported (16), DksA was completely inactive when its C-terminal α-helix (140–152) was removed. DksA(1–139) lacked both RNAP binding and functional activity in vitro (Fig. 5 *A* and *B* and *SI Appendix*, Figs. S4*A* and S5*A*) and activity in vivo (Fig. 5*C* and *SI Appendix*, Figs. S6 and S7). Serial C-terminal truncations displayed a progressive loss of function in vitro and in vivo (*SI Appendix*, Figs. S4*A*, S5*A*, S6, and S7), which suggested multiple contacts between RNAP and this α-helix. We found two point mutants in the C-terminal α-helix that exhibited functional defects. DksA-E143A significantly reduced the binding and activity of DksA in vitro, and DksA-K147A had smaller, but similar, effects (Fig. 5*B* and *SI Appendix*, Figs. S4*B* and S5*B*). Of these two point mutants, only DksA-E143A was defective in inhibiting transcription from *rrnBP1* in vivo (Fig. 5*C*), and both strains grew on minimal medium (*SI Appendix*, Fig. S7 and Table S2). The smaller effects seen with single substitutions are consistent with multiple sites across the C-terminal α-helix additively contributing to binding. In our model, DksA-E143 is positioned to interact with the tip of the β' rim helices (Fig. 3*B*), whereas DksA-K147 is distal to the β' rim helices and may contribute to the binding interface with β-SI1.

We also used genetic tests to characterize the interaction between β-SI1 and DksA. We first used a hyperactive DksA mutant (DksA-N88I) that has both higher affinity for and activity on RNAP, allowing it to suppress the auxotrophy of a ppGpp^0 strain (19). We reasoned that DksA-N88I would also be sufficient to restore binding and activity to mutants in the proposed DksA–β-SI1 interface. As predicted, DksA-N88I partially suppressed the in vivo growth defects of *rpoB(ΔSI1)*, *rpoB(ΔSI1-1.2)* (Fig. 4*D*), and *dksA(1–139)* (*SI Appendix*, Fig. S7). DksA-N88I also suppressed the in vitro defect in activity for RNAPΔSI1-1.2 (Fig. 4*E* and *SI Appendix*, Table S1). We next used epistasis analysis to test whether DksA binding was the sole function of β-SI1. If so, an *rpoB(ΔSI1)ΔdksA* double mutant phenotype should have been equivalent to either single mutant alone. This epistatic relationship held for a positive control, *rpoC(E677G)*, known to interfere with DksA binding (17) (*SI Appendix*, Fig. S8). In contrast, both *rpoB(ΔSI1)Δdks*A and *rpoB(ΔSI1-1.2)ΔdksA* were synthetic sick in combination, showing an extended lag before any growth in minimal medium (*SI Appendix*, Fig. S8). These results further support the conclusion that mutations in the DksA–β-SI1 interface reduce binding and activity of DksA and, unexpectedly, show that β-SI1

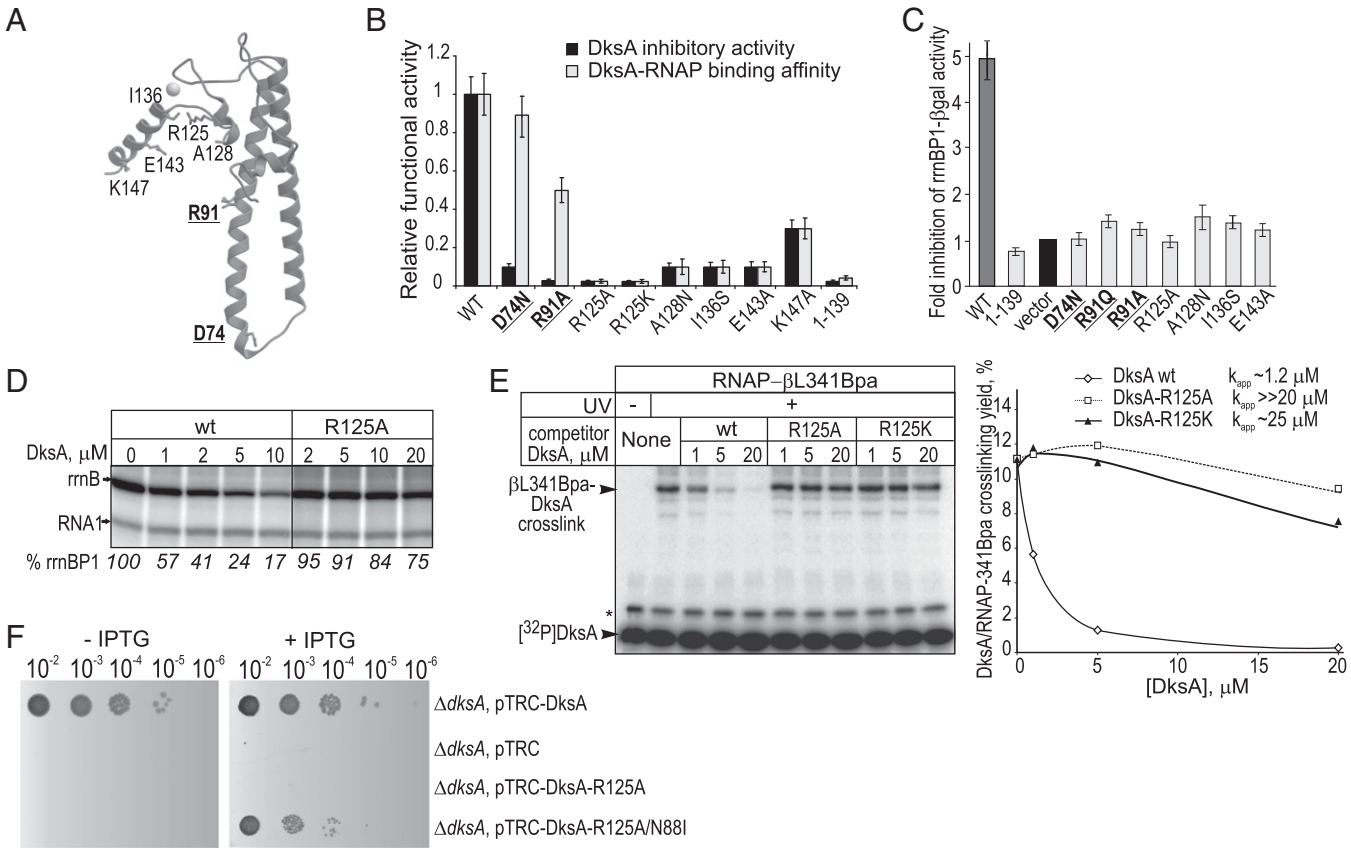

Fig. 5. Phenotypes of selected single-point DksA mutants with significant functional impairment. (*A*) Ribbon structure of *E. coli* DksA showing the position of critical residues (sticks). (*B*) Effect of mutations of critical residues in DksA on its binding affinity and ability to inhibit transcription from *rrnB-P1* in vitro. Data are plotted relative to activity of WT DksA; error bars represent SD ($n = 3$). In *B* and *C*, mutations resulting in significant reduction of DksA activity, but not binding affinity, are shown in bold typeface and are underlined. (*C*) In vivo transcriptional inhibitory activity of these same mutants measured as fold inhibition of an *rrnB* P1-lacZ fusion reporter during the stationary phase in *E. coli ΔdksA* cells expressing either plasmid-born WT or mutant DksA (upon induction with 1 mM IPTG). Data are plotted relative to that of ΔdksA cells (strain RLG7241) carrying the empty vector. (*D*) Multiround runoff transcription assays (as in Fig. 4*A*) comparing the concentration dependence of WT and R125 DksA for inhibition of *rrnB-P1* transcription. (*E*) Analysis of the binding affinity of DksA-R125 to RNAP with a competition–cross-linking assay. (*Left*) Autoradiogram of 6–12% SDS/PAGE of RNAP-βL341Bpa photo–cross-linked to radioactive WT DksA in the presence of various amounts of competitor DksA (WT or mutant) as indicated. Radiolabeled PKA present in the reaction mix is indicated by an asterisk. (*Right*) Quantification of the effect of mutant DksA concentration on the yield of RNAP–DksA cross-linking from which k_{app} is calculated. (*F*) Growth complementation assay showing that upon IPTG induction, plasmid-expressed DksA-R125A/N88I, but not DksA-R125A, rescues the auxotrophy of *E. coli ΔdksA* cells (strain CF9240) during 24 h of growth on M9 minimal agar plates at 30 °C. The serial dilution factor is indicated above.

contributes to growth on minimal media even in the absence of DksA.

In summary, multiple lines of evidence indicate that DksA and β-SI1 interact and that this interaction is critical for high-affinity binding of DksA to the initiation complex. This includes reciprocal cross-linking between DksA and β-SI1, the position of the C-terminal α-helix of DksA near β-SI1 in our model, and genetic validation of both sides of this interface.

The Tip of the β′ Rim Helices Binds the Zn^{2+}-Binding Domain and Adjacent C-Terminal α-Helix. The model predicted that the Zn^{2+}-binding domain of DksA (G112-K139) contacted the tip of the β′ rim helices (β′670–674) (Fig. 3*B*), a feature of RNAP that is known to be critical for DksA binding (12, 16, 20). Multiple mutations in both sides of the proposed interface identify key residues that contribute to DksA-binding affinity.

DksA-R125A (Fig. 5*A*) was the most defective point mutant in DksA. The mutant lacked both binding and activity in vitro (Fig. 5 *B*, *D*, and *E*), was unable to inhibit *rrnBP1* transcription in vivo, and did not support growth on minimal media (Fig. 5 *C* and *F*). Even the more conservative substitution, DksA-R125K, resulted in a nearly complete loss of RNAP binding (>20-fold decrease; Fig. 5*E*). Loss of activity was suppressed in a DksA-R125A/N88I double mutant strain, consistent with the phenotype being due to a lack of binding (Fig. 5*F*).

Two other residues in the Zn^{2+}-binding domain (A128 and I136) were also important for DksA function. DksA-A128N and DksA-I136S were defective for both binding and activity in vitro (Fig. 5*B* and *SI Appendix*, Figs. S4*B* and S5*B*) and inhibited expression from *rrnB* P1 very poorly in vivo (Fig. 5*C*). However, like the partially defective mutants of the β-SI1–DksA interface, they were able to support growth without added amino acids (*SI Appendix*, Fig. S7). A combination of DksA-E143A with these partially defective mutants (DksA-I136S/E143A and DksA-A128N/I136S/E143A) could not support growth without amino acids (*SI Appendix*, Fig. S7), suggesting that combining these weaker mutations can have a synergistic effect on DksA binding.

In the model, DksA-R125 is positioned to interact with β′-E677 (Fig. 3*B*), DksA-A128 and DksA-I136 are positioned to interact with the two aliphatic side chains in the tip of the rim helices (Fig. 3*B*), and DksA-E143 is positioned to interact with tip residue β′ T674. Although the atomic-level resolution of this interaction remains to be determined, we note that structural modeling and mutagenesis together implicate a direct interaction between the

Zn^{2+}-binding region of DksA and the tip of the β' rim helices. Functional analysis indicates that DksA-R125 is a major contributor to the binding energy of this interface. It is interesting to note that although the majority of residues implicated in our model are conserved, both DksA-R125 and β'-E677 are invariant across bacterial phyla (*SI Appendix*, Table S4), possibly reflecting a conserved salt bridge critical for DksA function.

The Coiled-Coil Tip of DksA Interacts with Residues in the Substrate-Binding Region of the Active Site. Identifying the position of the coiled-coil tip of DksA within the active-site region of RNAP is critical for understanding the mode of action of DksA. In our model, tip residue D74, one of the first to be identified as essential for DksA activity (3), is positioned to contact two residues of the substrate-binding site in the β subunit, β-R678 and β-R1106 (Figs. 2*E* and 3*C*). This assignment is supported by cross-linking between DksA-V73 and the overlapping region (β653–681) as well as functional analysis of mutants in D74, β-R678, and β-R1106.

We found that DksA-D74 substitutions D74N, D74S, and D74E all altered DksA activity without affecting binding, consistent with previous studies (3, 12, 21) (Fig. 5*B* and *SI Appendix*, Fig. S5*B*). D74N was the most defective of the substitutions (Fig. 5*C* and *SI Appendix*, Fig. S7 and Table S1). This suggested that proper positioning and electrostatic charge of the aspartic acid carboxyl group are critical for D74 function.

The two residues in β (R678 and R1106) proposed to interact with DksA-D74 each play important roles in catalytic function during elongation. β-R678 binds to the nascent RNA 3′-end and orients it for nucleotide addition, and β-R1106 stabilizes the incoming NTP (22, 23). RNAP complexes with alanine substitutions at either residue retained DksA affinity (*SI Appendix*, Fig. S9*B*) but were refractory to DksA inhibition in in vitro transcription assays, even at the concentrations 10-fold higher than that required for WT RNAP (Fig. 6*A*). A complementary assay based on destabilization of RPo by DksA at the model promoter lacUV5 DNA (24) also indicated that these mutants were refractory to DksA action: Although RNAP-βR678A and RNAP-βR1106A exhibited shorter half-lives than WT, they were insensitive to DksA-mediated destabilization (Fig. 6*B*). Substitution of the neighboring residues, β-N677A and β-S1105A, did not affect RNAP sensitivity to DksA (*SI Appendix*, Fig. S9*A*), indicating that the effects observed with β-R678A and β-R1106A were specific.

The observations that DksA-D74 exhibits charge complementarity with β-R678 and β-R1106, that mutation of these residues abrogates DksA function, and that all three residues are highly conserved among different bacterial phyla (*SI Appendix*, Table S5) together suggest that DksA-D74 forms a salt bridge with β-R678 and β-R1106 that is essential for DksA activity. We note that the proposed interaction of DksA-D74 with the substrate-binding region of the active site places DksA-A76 tightly against β'G782/L783 from the bridge helix. This provides an alternative explanation for the functional defects discovered for DksA-A76T, in that a steric clash from the bulky substitution would prevent DksA from inserting into the substrate-binding region of the active site (21).

A Novel DksA Coiled-Coil–β' Rim Helix Functional Interaction. Interestingly, we found that substitutions in DksA-R91 eliminate the activity of DksA and reduce, but do not eliminate, DksA binding (Fig. 5 *B* and *C* and *SI Appendix*, Figs. S4 *B* and *C*, S5*B*, and S7 and Table S2). This indicated that DksA-R91 is essential for DksA activity independent of binding, similar to the phenotype of the tip residue D74. The model positions DksA-R91 near β'-D684 (Fig. 3*D*), and substitution of β'-D684 also reduced the sensitivity of mutant RNAP to DksA in vitro (*SI Appendix*, Table S1). Compared with other proposed interaction interfaces, both DksA-R91 and the residues centered at β'-D684 are less conserved between phyla (*SI Appendix*, Table S5). We propose that an interaction between DksA-R91 with the β' rim helix stabilizes the orientation of the DksA coiled-coil that allows an interaction between DksA-D74 and the substrate-binding region of the active site.

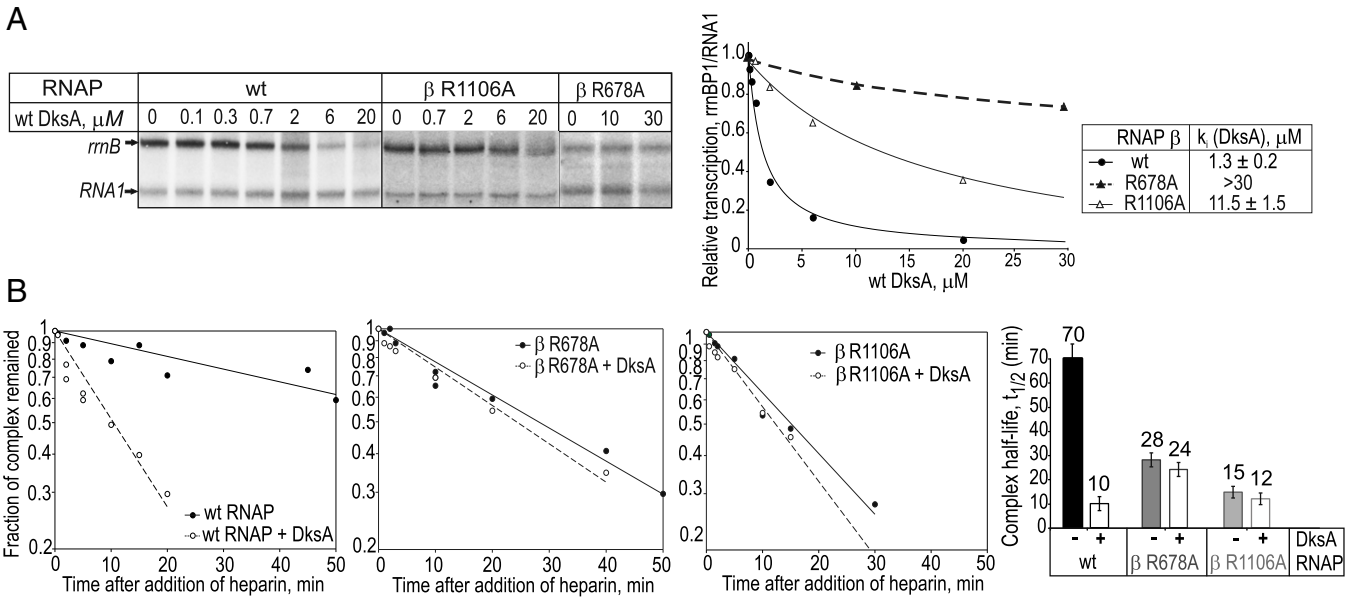

Fig. 6. Susceptibility of the RNAP β active-site region mutants, β-R678A and β-R1106A, to DksA inhibition. (*A*) Multiround transcription assays comparing the concentration dependence of DksA inhibition of rrnB-P1 for WT, β-R678A, or β-R1106A RNAP (*Left*), with quantification and the calculated k_i shown (*Right*) (*B*) Effect of 5 μM DksA on the lifetime of *lacUV5* open promoter complexes formed by WT, β-R678A, and β-R1106A RNAPs, measured by DNA filter binding (24). The decay curves show the fraction of complexes remaining at the indicated times after heparin addition. Bar graph indicates the half-lives calculated from these data.

Discussion

We present a new evidence-based model of the DksA–RNAP complex that highlights a dispersed network of mutually dependent interactions required for both binding and activity of DksA. High-affinity binding requires an interaction between β-SI1 and the C-terminal α-helix of DksA as well as between the tip of the β' rim helices and the Zn^{2+}-binding region of DksA. Eliminating either interaction alone abolished binding, showing that both the β' rim helices and β-SI1 are necessary binding determinants of DksA.

DksA and β-SI1 are too distant to physically interact in our model, which is based on DksA and RNAP crystallized independently. The DksA C-terminal α-helix and β-SI1 both display conformational flexibility (by 7–15 Å) based on the reported crystal structures of DksA [Protein Data Bank (PDB) ID codes 1TJL and 4IJJ] and RNAP (PDB ID codes 4LK1, 4YLN, and 4JKR). The movement of the two domains toward each other by 5–10 Å and 10–15 Å, respectively, could easily bring β-SI1 close enough to interact with DksA. DksA binding could thus capture an alternative conformation to that found in the crystal structure of *E. coli* RNAP (23, 25–28) and compete with any function of β-SI1 associated with this original conformation. Although we have clearly demonstrated that β-SI1 recruits DksA to RNAP, further efforts both to dissect this novel binding interface and to characterize the DksA-independent functions of β-SI1 will be critical for completing the picture of how the interaction between β-SI1 and DksA alters transcription.

Our work has revealed that the residues in the β substrate-binding region of the active site are required for sensitivity to DksA during initiation. We propose that DksA-D74 functions during initiation by neutralizing the positive charges of β-R678/R1106 and altering the dense network of polar–electrostatic interactions in the immediate vicinity of the active center (23, 26, 28, 29). This could alter the conformation of two neighboring mobile elements of β, fork loop-1 and fork loop-2, destabilizing the intermediate on the pathway to open complex formation. Alternatively, the β' trigger loop (β' TL) has been previously demonstrated to be essential for sensitivity to DksA (7, 20). Our model predicts a steric clash between a folded β' TL and the coiled-coil of DksA, and an alternative mechanistic role of both DksA-D74 and DksA-91 could be to lock the coiled-coil in the appropriate orientation to mediate this interaction. Regardless of exact conformational changes that destabilize RPi, we have provided strong evidence that an interaction between the substrate-binding region of the active site and DksA-D74 is a critical feature of DksA regulation during initiation.

DksA is known to alter the elongation properties of RNAP (3, 20, 30), and we note that DksA statically bound to RNAP as found in our model would preclude elongation by preventing folding of the β' TL. Our experimental efforts focused on the effects of DksA during initiation, but the position of the DksA coiled-coil in the channel may be dynamic and vary with RNAP conformation, the stage of transcription cycle, and the presence of additional factors such as ppGpp. Indeed, Fe^{2+}-mediated cleavage of DksA is reduced for nonfunctional DksA-tip mutants (21), and in the paused complex as compared to free RNAP (20). This reduced cleavage has been interpreted as representing a more distal position of the coiled-coil in the these complexes (20). One alternative model positions DksA so that binding would not clash with a folded β' TL and may represent a more relevant mode of binding during elongation (12).

For *E. coli* RNAP, DksA binding is modulated by two lineage-specific insertions: β-SI1 and β'-SI3. Although β'-SI3 antagonizes DksA binding and is hypothesized to contribute to the steric clash between DksA and a folded β' TL (16), β-SI1 is essential for recruiting DksA to RNAP. This discovery has interesting implications for the conservation of DksA regulation among diverse bacteria. Like β'-SI3 (16), β-SI1 cooccurs with DksA, present in 22/25 of the bacterial phyla with DksA homologs (*SI Appendix*, Table S3). In most DksA-containing phyla, β-SI1 is present either as a full-length domain (containing all three proposed interacting loops) or as a short insertion containing only loop 1. In phyla with a truncated β-SI1, features of DksA may have evolved to compensate for this loss and maintain a high-binding affinity. For example, five phyla that carry a truncated β-SI1 also have an extended C-terminal α-helix in DksA (*SI Appendix*, Table S3). Comparing the regulatory capabilities of DksA in these bacteria to those of *E. coli* would indicate the diversity of mechanisms that have evolved to allow for control of transcription by DksA.

Materials and Methods

Strains, Oligos, and Growth Conditions. *E. coli* strains and plasmids are listed in *SI Appendix*, Table S6. Primers used in all PCR-based cloning were obtained from Integrated DNA Technologies; their sequences are available upon request. Deletions, single- and multiple-point mutations, and amber codon (UAG) substitutions were introduced at various positions within the *dksA*, *rpoB*, and *rpoC* genes using the QuikChange site-directed mutagenesis kit (Agilent). Chromosomal mutants in *rpoB* and *dksA* were generated by oligo-mediated recombineering using the λ-red system and standard protocols (31). Colony size estimations were made on arrayed colonies on agar plates using the same methodology as previously described for large-scale chemical-genomic screens (32).

Expression and Purification of Mutant DksA and RNAP Proteins. Bpa-substituted variants of DksA and RNAP were prepared using *E. coli* BL21(DE3) and CAG316 cells, respectively. Strains were cotransformed with a Bpa-specific evolved tRNA/tRNA synthetase pEVOL-BpF vector (33) and the appropriate expression plasmid (*SI Appendix*, Table S6). Transformants were grown to an OD_{600} ~0.5–0.6 at 30 °C in liquid LB media supplemented with ampicillin (100 μg/mL) and chloramphenicol (30 μg/mL). Protein expression was induced by addition of 1 mM Bpa, 1 mM isopropyl β-D-1-thiogalactopyranoside (IPTG), and 0.02% arabinose to the growth media, and the induced cells were grown for ~20 h at 30 °C. DksA-Bpa and RNAP-Bpa proteins were purified under reduced light at 4 °C by Ni^{2+}-chelating nitrilotriacetic acid agarose (NTA-agarose) (Qiagen) followed by size-exclusion chromatography on Superdex 75 and Superose 6 (GE Healthcare Life Sciences), respectively (34). Other mutant DksA and RNAP proteins were expressed using the same strains (without cotransformation with pEVOl-BpF) and purified as described above.

Protein Cross-Linking and Mapping. A purified RNAP core enzyme carrying either N- or C-terminal PKA- and 6xHis-tag (NPH or CPH, respectively) on β' or β subunits was radiolabeled using [γ-^{32}P]-ATP (3,000 Ci/mmol; MP Biomedicals) and protein kinase A (PKA; New England Biolabs) as described previously (34). Cross-linking reactions were initiated by mixing 0.5 μM [α-^{32}P]–RNAP with 0.5–2 μM DksA-Bpa in 15 μL reaction buffer (40 mM Tris·HCl pH 7.9, 50 mM NaCl, 10 mM $MgCl_2$, and 0.2 mg/mL BSA) followed by irradiation by a 365-nm UV lamp for 20 min at 4 °C. The reaction was terminated by addition of 3 μL of 5× SDS sample loading buffer containing β-mercaptoethanol. The cross-linked products were separated by 6% (wt/vol) Tris-glycine SDS polyacrylamide gel electrophoresis (SDS/PAGE), visualized by autoradiography, and quantified by PhosphorImager (GE Healthcare Life Sciences). The results of the cross-linking experiments were essentially the same when RNAP σ70-holoenzyme was used instead of the core enzyme. The free radiolabeled β and β' and their covalent adducts carrying DksA-Bpa were excised from the gel and eluted with three volumes of 0.2% SDS at room temperature for 1 h. The eluate was precipitated by acetone and redissolved in 20 μL of 0.1% SDS and then directly used in cleavage reactions.

Mapping of the cross-linked sites on β and β' was performed by limited chemical or enzymatic hydrolysis under single-hit conditions. Chemical hydrolysis was initiated by mixing the eluted radioactive material with 40 mM HCl and 40 mM BrCN in 10 μL of 0.2% SDS followed by incubation at 30 °C for 5–30 min. The reaction was terminated by addition of 0.5 μL of 1 M Tris–OH. Enzymatic cleavage was performed by mixing the eluted radioactive material with 1 μg unlabeled RNAP and 1–10 ng trypsin (Thermo Fisher Scientific Inc.) in 15 μL of buffer (100 mM Na-phosphate pH 7.0, 0.05% SDS) followed by incubation at 37 °C for 5–30 min. Reaction was terminated as described above, and the products of cleavage reactions were resolved by 7% or 10% (wt/vol) SDS/PAGE and visualized by PhosphoImager. Protein cleavages at Met and Arg/Lys residues were carried out as described (34, 35)

using BrCN and trypsin, respectively. Because the PKA sites are located at β and β′ polypeptide termini, the single-hit hydrolysis generates a pattern of nested, easily identifiable fragments.

Modeling of the DksA–RNAP Complex. Atomic-resolution representations of the structures of RNAP (PDB ID code 4LK1) and DksA (PDB ID code 1TJL-A) and the experimental cross-linking data were used as starting points for automated modeling. To account for ambiguous cross-linking data, our scoring function required that at least one possible cross-link criterion was satisfied (Cα–Cα distance < 20 Å) for each Bpa-replaced residue of DksA (57, 69, 73, 79, 84, 119, 140, 144, and 148) that had a corresponding RNAP fragment in the structural model (Fig. 2*E* and *SI Appendix*, Fig. S3). Because the β′-SI3 domain is highly flexible, as found in several RNAP crystal structures (PDB ID codes 4LK1, 4LK0, 4JKR, 4IQZ, and 4YLN), the cross-link from DksA-E146Bpa was excluded from this initial analysis. Sampling of models with good shape complementarity using the PatchDock method generated ∼130,000 docking models. This set was then filtered using a cross-linking scoring function. Preliminary analysis revealed that none of the ∼130,000 docking models satisfied all 10 cross-links. However, exclusion of DksA-V119 and satisfaction of the remaining nine cross-links filtered the set to two clusters of models (model 1, yellow ribbons; model 2, blue ribbons; *SI Appendix*, Fig. S3*E*). The model that had the most favorable shape complementarity score and also satisfied the distance interaction criteria between DksA and the tip of the β′ rim helices (model 2) was used for further refinement.

First, for the refined modeling, predicted positions of β′-SI3 in the RNAP structure (PDB ID codes 4JKR, 4YLN, and 4LJZ) were used to put an additional constraint to possible positions of DksA in the secondary channel. At the same time, the potential steric clash that may occur between the N-terminal partially unstructured region of DksA (residues 1–13) and β′ rim helices was allowed. Second, only the cross-links from DksA-Bpa residues 57, 69, 73, and 84 to stationary β and β′ structural elements (36) were used, because they allowed a more unambiguous placement of DksA. The cross-linking data from other DksA-Bpa residues were excluded from the analysis, as the cross-links were mapped to mobile structural elements (β′-TL, β′-SI3, β-SI1, and β-lobe 1). Third, we used additional experimental data resulting from the functional analysis of ≥30 DksA mutants (*SI Appendix*, Figs. S4–S7). Among these were the *N*- and C-terminal deletions (*SI Appendix*, Figs. S4*A*, S5*A*, and S6) and point mutations at or near the six residues for which Bpa substitutions did not appreciably cross-link to RNAP (Fig. 2*C*). We reasoned that these surface-exposed substitutions were unlikely to alter folding and may identify critical binding interfaces that are unable to tolerate the bulky Bpa adduct. The latter group of mutants proved to be the most informative for the refined modeling, as substitutions of R91, R125, A128, I136, E143, and K147 were most detrimental for binding and/or activity (Fig. 5 and *SI Appendix*, Figs. S4 *B* and *C* and S5*B*). In the final DksA model (*SI Appendix*, Fig. S3*E*, model 3, red ribbons), the coiled-coil and Zn^{2+}-binding domains are positioned closer to β′ rim helices than that observed in model 2. As a result, the side chains of possible cross-linked residues (of DksA and RNAP) are located at interacting distances of <4 Å.

DNA Filter Binding Assay. The lifetimes of a competitor-resistant RNAP–promoter complex were measured in a DNA filter-binding assay, as described (24). The fraction of competitor-resistant RNAP–promoter complex remaining in either the absence or presence of DksA was measured by a DNA filter-binding assay using a 242-bp-long end-radiolabeled DNA fragment containing the *lacUV5* promoter (endpoints –60 to +40) prepared by filling in the ends of XhoI-digested pRLG4264 plasmid with [α-^{32}P] TTP (MP Biomedicals) and Sequenase (USB). For the assay, 10–30 nM RNAP was mixed with 0.5 nM radiolabeled *lacUV5* DNA and 5 μM DksA in binding buffer (40 mM Tris·Cl pH 7.9, 100 mM NaCl, 10 mM $MgCl_2$, 1 mM DTT, and 0.1 mg/mL BSA) and incubated at 30 °C for 20 min. After addition of heparin (Sigma) to 10 μg/mL, 20 μL aliquots were removed from the mixture at indicated time intervals and filtered through nitrocellulose discs (Protran BA-85; Whatman). The discs were washed (2 × 200 μL) with 10 mM Tris·HCl buffer pH 8.0 containing 100 mM NaCl and 0.5 mM EDTA, air-dried, and quantified by scintillation counter (Beckman). RNAP–promoter complex half-lives were determined from semilog linear regression plots of the fraction of filter-retained complex at each time point. Time 0 was defined as 15 s after heparin addition in the absence of DksA.

β-Galactosidase Activity Assay. β-galactosidase activity was measured for WT and mutant *E. coli* strains containing a chromosomal *rrnB* P1 promoter-lacZ fusion reporter, as described (24), after growth to stationary phase in M9 rich defined media (M9-RDM) to an OD_{450} of 1.0–2.2 or in LB to an OD_{600} of ∼5.5.

To measure the β-galactosidase activity of chromosomally expressed mutant RNAPs, cells from fresh single colonies were grown in M9-RDM into the stationary phase for 24 h at 30 °C (to an OD_{450} of 1.0–2.2). Cultures were placed on ice for 30 min and diluted 1:10 in ice-cold Z-buffer (60 mM sodium phosphate buffer pH 7.0, 13 mM NaCl, and 1 mM Mg_2SO_4). Reaction mixtures were prepared by mixing 500 μL of the culture dilution, 500 μL lysis buffer [Z-buffer containing 0.006% (wt/vol) SDS, 38 mM β-mercaptoethanol], and 50 μL of chloroform and vortexing for 10 s. Reactions were initiated by addition of 200 μL of 4 mg/mL *o*-nitrophenyl-β-galactoside (ONPG), incubated for 7–30 min at 25 °C, and quenched with 500 μL of 1 M $NaHCO_3$.

To measure the β-galactosidase activity in cells expressing mutant DksA, an *E. coli ΔgreA:ΔdksA* double mutant strain (RLG7241) carrying chromosomal *rrnB* P1 promoter-lacZ fusion was transformed with pTRC99A-derived vectors expressing the WT or mutant DksA. The double deletion strain was used to minimize the interference effect of competitor GreA on DksA activity (6). Cells were grown in triplicates in LB media in the presence of 1 mM IPTG and 100 mg/mL ampicillin for 24 h at 30 °C to an OD_{600} of ∼5.5 (stationary phase). We centrifuged 50 μL of cell aliquots and placed them on ice for ∼20 min. Cells were resuspended in 100 μL of lysis buffer (100 mM Na_2HPO_4, 20 mM KCl, 2 mM $MgSO_4$, 0.8 mg/mL cetrimonium bromide, 0.4 mg/mL Na-deoxycholate, 80 mM β-mercaptoethanol, and 100 μg/mL chloramphenicol) and lysed by sonication. We added 300 μL of substrate solution (60 mM Na_2HPO_4, 40 mM NaH_2PO_4, 1 mg/mL ONPG, and 13 mM β-mercaptoethanol) to the lysate and incubated it for 15–30 min at 37 °C. The reaction was quenched as above, and the OD_{420} was measured. The β-galactosidase activity was calculated in Miller Units using the following equation: $(1{,}000 \times OD_{420})/(OD_{600} \times 0.1 \times t)$, where OD_{420} is optical density of the supernatant at 420 nm, OD_{600} is optical density of the cell suspension before lysis at 600 nm, and t is the reaction time in minutes.

In Vitro Transcription Assays. To measure the inhibitory effect of DksA on RNAP transcription from ribosomal *rrnB* P1 promoter DNA, a multiround in vitro transcription assay was performed as described (2) using 40 ng of supercoiled plasmid pRLG862 (carrying *rrnB* P1 promoter with endpoints –88 to +50 relative to the transcription start site) mixed with 30 nM RNAP incubated in 10 μL of transcription buffer (40 mM Tris·HCl pH 7.9, 140 mM NaCl, 10 mM $MgCl_2$, 1 mM DTT, and 0.1 mg/mL BSA) in the presence or absence of 0.2–35 μM of WT or mutant DksA at 30 °C for 5 min. Reactions were initiated by addition of NTPs (200 μM each of ATP, GTP, and CTP; 10 μM UTP; and 1 μCi [α-^{32}P]UTP) followed by incubation at 30 °C for 10 min. Reactions were terminated with 15 μL of RNA gel loading buffer (95% formamide, 20 mM EDTA, 0.05% bromophenol blue, and 0.05% xylene cyanol), and the RNA products were separated on denaturing 8% PAGE in the presence of 7 M urea and quantified by PhosphorImager with ImageQuant.

DksA–RNAP-Binding Assays. To assess the binding affinities of mutant RNAPs toward the WT DksA, a direct photo–cross-linking (DksA-Bpa.RNAP) assay was used. A mixture of 10–30 nM of radiolabeled DksA-L84Bpa (or DksA-R87Bpa) and 30–900 nM RNAP in 15 μL of transcription buffer was UV-irradiated at 365 nm for 5 min at 4 °C. The reaction was terminated by addition of 4 μL of 5× SDS sample loading buffer, and the cross-linked products were separated by 12% Tris–glycine SDS/PAGE, visualized by autoradiography, and quantified by PhosphorImager (GE Healthcare Life Sciences). The apparent dissociation constant (K_d) was calculated from the graphs as the concentration of RNAP that yields half-maximum efficiency of cross-linking to DksA-Bpa. To determine the binding affinities of mutant DksA toward the WT RNAP, an indirect competition–cross-linking (DksA-Bpa/mutant DksA/RNAP) assay was used. An equimolar mixture of 50 nM radiolabeled DksA-L87Bpa and WT RNAP (or radiolabeled WT DksA and RNAP-β-L341Bpa) was incubated in the presence of 0–30 μM of unlabeled WT or mutant DksA used as a competitor in 15 μL of transcription buffer for 15 min at 4 °C. Reactions were UV-irradiated, analyzed by SDS/PAGE, and quantified as described above. The apparent relative dissociation constant (K_{app}) was calculated from the graphs as the concentration of competitor DksA that causes a 50% decrease in the cross-linking efficiency between radiolabeled DksA and RNAP.

ACKNOWLEDGMENTS. We thank R. Gourse, W. Ross, C. Herman, and M. Cashel for kindly providing strains and plasmids and for their helpful comments. We also thank P. Schultz for providing the pEVOL-BpF plasmid. This work was supported by National Institutes of Health Grants R01GM057755 and R01GM102790 (to C.A.G.) and by the University of Medicine and Dentistry of New Jersey (UMDNJ) Foundation for Research (to S.B.). This research was also supported in part by an award from the Department of Energy Office of Science Graduate Fellowship Program (to A.L.S.).

1. Braeken K, Moris M, Daniels R, Vanderleyden J, Michiels J (2006) New horizons for (p)ppGpp in bacterial and plant physiology. *Trends Microbiol* 14(1):45–54.
2. Paul BJ, et al. (2004) DksA: A critical component of the transcription initiation machinery that potentiates the regulation of rRNA promoters by ppGpp and the initiating NTP. *Cell* 118(3):311–322.
3. Perederina A, et al. (2004) Regulation through the secondary channel—Structural framework for ppGpp-DksA synergism during transcription. *Cell* 118(3):297–309.
4. Dalebroux ZD, Svensson SL, Gaynor EC, Swanson MS (2010) ppGpp conjures bacterial virulence. *Microbiol Mol Biol Rev* 74(2):171–199.
5. Haugen SP, Ross W, Gourse RL (2008) Advances in bacterial promoter recognition and its control by factors that do not bind DNA. *Nat Rev Microbiol* 6(7):507–519.
6. Vinella D, Potrykus K, Murphy H, Cashel M (2012) Effects on growth by changes of the balance between GreA, GreB, and DksA suggest mutual competition and functional redundancy in Escherichia coli. *J Bacteriol* 194(2):261–273.
7. Rutherford ST, Villers CL, Lee J-H, Ross W, Gourse RL (2009) Allosteric control of Escherichia coli rRNA promoter complexes by DksA. *Genes Dev* 23(2):236–248.
8. Bartlett MS, Gaal T, Ross W, Gourse RL (1998) RNA polymerase mutants that destabilize RNA polymerase-promoter complexes alter NTP-sensing by rrn P1 promoters. *J Mol Biol* 279(2):331–345.
9. Trautinger BW, Lloyd RG (2002) Modulation of DNA repair by mutations flanking the DNA channel through RNA polymerase. *EMBO J* 21(24):6944–6953.
10. Dormán G, Prestwich GD (1994) Benzophenone photophores in biochemistry. *Biochemistry* 33(19):5661–5673.
11. Forné I, Ludwigsen J, Imhof A, Becker PB, Mueller-Planitz F (2012) Probing the conformation of the ISWI ATPase domain with genetically encoded photoreactive crosslinkers and mass spectrometry. *Mol Cell Proteomics* 11(4):M111.012088.
12. Lennon CW, et al. (2012) Direct interactions between the coiled-coil tip of DksA and the trigger loop of RNA polymerase mediate transcriptional regulation. *Genes Dev* 26(23):2634–2646.
13. Laptenko O, Borukhov S (2003) Biochemical assays of Gre factors of Thermus thermophilus. *Methods Enzymol* 371:219–232.
14. Mustaev A, et al. (2003) Strategies and methods of cross-linking of RNA polymerase active center. *Methods Enzymol* 371:191–206.
15. Schneidman-Duhovny D, et al. (2012) A method for integrative structure determination of protein-protein complexes. *Bioinformatics* 28(24):3282–3289.
16. Furman R, Tsodikov OV, Wolf YI, Artsimovitch I (2013) An insertion in the catalytic trigger loop gates the secondary channel of RNA polymerase. *J Mol Biol* 425(1):82–93.
17. Satory D, Halliday JA, Sivaramakrishnan P, Lua RC, Herman C (2013) Characterization of a novel RNA polymerase mutant that alters DksA activity. *J Bacteriol* 195(18):4187–4194.
18. Rutherford ST, et al. (2007) Effects of DksA, GreA, and GreB on transcription initiation: Insights into the mechanisms of factors that bind in the secondary channel of RNA polymerase. *J Mol Biol* 366(4):1243–1257.
19. Blankschien MD, et al. (2009) Super DksAs: Substitutions in DksA enhancing its effects on transcription initiation. *EMBO J* 28(12):1720–1731.
20. Furman R, Sevostyanova A, Artsimovitch I (2012) Transcription initiation factor DksA has diverse effects on RNA chain elongation. *Nucleic Acids Res* 40(8):3392–3402.
21. Lee J-H, Lennon CW, Ross W, Gourse RL (2012) Role of the coiled-coil tip of Escherichia coli DksA in promoter control. *J Mol Biol* 416(4):503–517.
22. Holmes SF, Santangelo TJ, Cunningham CK, Roberts JW, Erie DA (2006) Kinetic investigation of Escherichia coli RNA polymerase mutants that influence nucleotide discrimination and transcription fidelity. *J Biol Chem* 281(27):18677–18683.
23. Vassylyev DG, et al. (2007) Structural basis for substrate loading in bacterial RNA polymerase. *Nature* 448(7150):163–168.
24. Barker MM, Gaal T, Josaitis CA, Gourse RL (2001) Mechanism of regulation of transcription initiation by ppGpp. I. Effects of ppGpp on transcription initiation in vivo and in vitro. *J Mol Biol* 305(4):673–688.
25. Saecker RM, Record MT, Jr, Dehaseth PL (2011) Mechanism of bacterial transcription initiation: RNA polymerase-promoter binding, isomerization to initiation-competent open complexes, and initiation of RNA synthesis. *J Mol Biol* 412(5):754–771.
26. Murakami KS (2013) X-ray crystal structure of Escherichia coli RNA polymerase σ70 holoenzyme. *J Biol Chem* 288(13):9126–9134.
27. Bae B, et al. (2013) Phage T7 Gp2 inhibition of Escherichia coli RNA polymerase involves misappropriation of σ70 domain 1.1. *Proc Natl Acad Sci USA* 110(49):19772–19777.
28. Zuo Y, Steitz TA (2015) Crystal structures of the E. coli transcription initiation complexes with a complete bubble. *Mol Cell* 58(3):534–540.
29. Darst SA, et al. (2002) Conformational flexibility of bacterial RNA polymerase. *Proc Natl Acad Sci USA* 99(7):4296–4301.
30. Zhang Y, et al. (2014) DksA guards elongating RNA polymerase against ribosome-stalling-induced arrest. *Mol Cell* 53(5):766–778.
31. Sharan SK, Thomason LC, Kuznetsov SG, Court DL (2009) Recombineering: A homologous recombination-based method of genetic engineering. *Nat Protoc* 4(2):206–223.
32. Nichols RJ, et al. (2011) Phenotypic landscape of a bacterial cell. *Cell* 144(1):143–156.
33. Young TS, Ahmad I, Yin JA, Schultz PG (2010) An enhanced system for unnatural amino acid mutagenesis in E. coli. *J Mol Biol* 395(2):361–374.
34. Laptenko O, Lee J, Lomakin I, Borukhov S (2003) Transcript cleavage factors GreA and GreB act as transient catalytic components of RNA polymerase. *EMBO J* 22(23):6322–6334.
35. Mustaev A, et al. (1997) Modular organization of the catalytic center of RNA polymerase. *Proc Natl Acad Sci USA* 94(13):6641–6645.
36. Borukhov S, Nudler E (2008) RNA polymerase: The vehicle of transcription. *Trends Microbiol* 16(3):126–134.
37. Borukhov S (2013) RNA polymerase structure, bacterial. *Encyclopedia of Biological Chemistry* (Academic, Waltham, MA), pp 173–184.